Acta Geotechnica (2017) 12:1415–1429
DOI 10.1007/s11440-017-0541-5

RESEARCH PAPER

Probabilistic evaluation of tunnel face stability in spatially random soils using sparse polynomial chaos expansion with global sensitivity analysis

Qiujing Pan[1] · **Daniel Dias**[1]

Received: 29 June 2016 / Accepted: 17 March 2017 / Published online: 27 March 2017

Abstract The sparse polynomial chaos expansion is employed to perform a probabilistic analysis of the tunnel face stability in the spatially random soils. A shield tunnel under compressed air is considered which implies that the applied pressure is uniformly distributed on the tunnel face. Two sets of failure mechanisms in the context of the limit analysis theory with respect to the frictional and the purely cohesive soils are used to calculate the required face pressure. In the case of the frictional soils, the cohesion and the friction angle are modeled as two anisotropic cross-correlated lognormal random fields; for the purely cohesive soils, the cohesion and the unit weight are modeled as two anisotropic independent lognormal random fields. The influences of the spatial variability and of the cross-correlation between the cohesion and the friction angle on the probability density function of the required face pressure, on the sensitivity index and on the failure probability are discussed. The obtained results show that the spatial variability has an important influence on the probability density function as well as the failure probability, but it has a negligible impact on the Sobol's index.

Keywords Limit analysis · Probabilistic analysis · Sensitivity analysis · Sparse polynomial chaos expansion · Spatial variability · Tunnel face stability

✉ Daniel Dias
daniel.dias@3sr-grenoble.fr

[1] Laboratory 3SR, CNRS UMR 5521, Grenoble Alpes University, Grenoble, France

1 Introduction

The assessment of the face stability is an important topic for the tunnel engineering. Many papers have been devoted to this topic in the last 20 years, aiming to develop calculation models to predict the necessary face pressure against failure. These deterministic models work well and require relevant input parameters, e.g., the soil strength properties, the unit weigh, the tunnel diameter [8, 26, 28, 38]. In practice, most of these required input parameters are generally not known exactly, subjected to different levels of uncertainty. Therefore, it is interesting to perform probabilistic analysis to account for the uncertainties of input parameters.

The probabilistic analysis has gained increased attention in the engineering design recently, as it is able to study the influence of uncertainties of input parameters in a rational way. Many attempts have been made to study the tunnel face stability from the probabilistic framework. Mollon et al. [23] performed a probabilistic analysis for a circular tunnel face stability using the first-order reliability method (FORM) based on the upper-bound limit analysis models, while Mollon et al. [24] conducted a probabilistic analysis on a face stability using the response surface method (RSM) in which both the ultimate limit state and the serviceability limit state were considered with the application of numerical deterministic models. Mollon et al. [25, 27] conducted a probabilistic analysis on the tunnel face stability using the collocation-based stochastic response surface methodology by which more input random variables, including the soil shear strength, the unit weight, the cover depth and the applied face pressure were involved. Zeng et al. [39] presented a reliability analysis on a rock tunnel face by means of the FORM, RSM and important sampling (IS). All these probabilistic studies provide more insight

than deterministic analysis and show the effectiveness and the necessity of the probabilistic analysis.

However, the aforementioned probabilistic analysis on the tunnel face stability regarded the input parameters as random variables, which failed to consider the inherent spatial variability of soil properties. It is well known in the geotechnical community that soils show obvious spatially variable properties. For example, soil properties change in both the vertical and the horizontal directions in situ. The random field theory is widely used to model the spatially variability of soil properties. Several methods such as the spatial average method, the midpoint method and the shape function method have been developed to discretize random fields in the last three decades. The efficiency of these approaches appears to be relatively low, as a large number of random variables are required for a prescribed accuracy [33]. The series expansion methods such as the Karhunen–Loeve (K–L) expansion or the expansion optimal linear estimation (EOLE) are more efficient approaches for random field discretization. The K–L expansion [10, 16] and EOLE [3] were adopted for the random field generation for the study of a slope stability and of a foundation bearing capacity. To the best of our knowledge, the existing probabilistic studies on the tunnel face stability only concern random variables; rare work has been done on tunnel face stability considering the soil spatial variability. The presented work aims to fill this gap; it is devoted to perform a probabilistic analysis on a tunnel face driven in spatially random soils.

Even though random fields could effectively model spatially varying soil properties, it often results in numerous variables in comparison with the simple random variable method, e.g., more than 100–200 variables, arising from the truncated terms of the expansion for a target accuracy. This feature often makes it difficult to conduct a probabilistic analysis with the random field model since most widely used reliability approaches, such as the first-order and second-order reliability method (FORM/SORM), the response surface method (RSM), are not able to handle too many random variables. Even though the classical Monte Carlo method is independent of the dimension of the input variables, it suffers from a quite low computational efficiency. To bypass this problem, a metamodel-based Monte Carlo method has been recently developed to perform probabilistic analysis. The procedure of this method is to firstly construct an analytical metamodel with a limited calls of the original model and secondly perform the Monte Carlo simulation based on this metamodel. The polynomial chaos expansion (PCE) is an efficient tool to build such an analytical metamodel. The PCE-based MC simulation was applied by many researchers to perform probabilistic analysis [14, 18–20, 22, 25, 32, 37]. However, the PCE-metamodel is unaffordable to build up for high-dimensional problems, like a random field with a fifth PCE, since the number of terms to be calculated rapidly increase with the number of the input variables and with the PCE order. In order to solve this problem, the sparse polynomial chaos expansion (SPCE) was proposed by Blatman and Sudret [5, 7] which results in a rather less PCE terms compared with that of the full PCE. An application of the SPCE to the bearing capacity of strip footings on spatially random soils can be found in Al-Bittar and Soubra [2, 3].

This work aims to perform a probabilistic analysis on the tunnel face stability in spatially random soils. The random field theory is used to model the spatial variability of the soil properties. The SPCE in combination with a global sensitivity analysis (GSA) is employed to implement the probabilistic analysis. The deterministic calculation of the required face pressure is based on the upper-bound limit analysis theory, in which two sets of failure mechanisms are, respectively, adopted to compute the face pressure in the frictional soils and in the purely cohesive soils. Finally, the probabilistic analysis is performed to discuss the influence of the autocorrelation distances and of the cross-correlation between c and φ on the probability density functions (PDF), on the sensitivity indices and on the failure probability.

2 Deterministic models for a tunnel face by the kinematic approach

In tunneling engineering, the shield machine can provide a support to the tunnel face, which is idealized as the distributed pressures applied to the tunnel face [8, 38]. This applied pressure is important to govern the tunnel face stability. If the applied pressure is not enough, the soils are about to move toward the tunnel face with ground surface subsidence, termed as the active collapse mode; if the applied pressure is overlarge, the soils will be heaved away the tunnel face with ground surface uplift, which is called as the passive blowout mode.

The issue of face stability has been widely investigated by means of the kinematic approach of limit analysis, in which the so-called failure mechanisms are developed to estimate the magnitude of the necessary face pressures against the tunnel face failures (collapse or blowout). The failure mechanisms are constructed according to the velocity field of soils ahead of the tunnel face at failure. For different failure modes (collapse or blowout), it is necessary to build different failure mechanisms because the soil movement is different between the collapse mode and the blowout mode. For different soils (the frictional soils and the purely cohesive soils), it is also necessary to construct different mechanisms even for the same failure mode because the failure feature of the soils is different. For

example, for the frictional soils there exists a thin shearing band at the failure surface, while for the purely cohesive soils, the soil deformation is continuous [28].

Many papers have been devoted to this topic in the last 20 years. The original work mainly lies in finding a more rational failure mechanism according to experimental investigations or numerical simulation. Two sets of original 3D failure mechanisms with respect to the frictional soils and the purely cohesive soils were proposed by Mollon et al. [26, 28]. Figure 1a shows a sketch of the rigid-block collapse mechanism for the frictional soil. This failure mechanism assumes a cylindrical rotational velocity field, rotating around a horizontal axis with an angular velocity. The velocity in the failure mechanism is equal to the product of the angular velocity and the distance between the rotating center and the point under consideration. The geometry of the failure mechanism is determined by the position of the rotation axis, leading to two parameters in the optimal process for the best upper-bound solutions. This classical collapse mechanism inspires a series of subsequent contributions [9, 29–31, 35].

The ground deformation around the tunnel face at failure in purely cohesive soils is different from that in the c–φ soils. The failure in purely cohesive soils involves a continuous deformation of the soil mass ahead of the tunnel face. Based on this observation, Mollon et al. [28] proposed two continuous velocity fields in terms of the collapse and the blowout of a tunnel face, as shown in Fig. 1b. The boundary of the mechanism resembles a torus, whose cross section is not strictly circular. The normality which states that any plastic deformation happens at constant volume in the non-frictional soil is used to determine the velocity field, which is equal to zero at the boundary (no velocity jump).

Each set of failure mechanisms concerns two failure modes, the active collapse mode (the applied face pressure is too small) and the passive blowout mode (the applied face pressure is too large) at the tunnel face. For the active

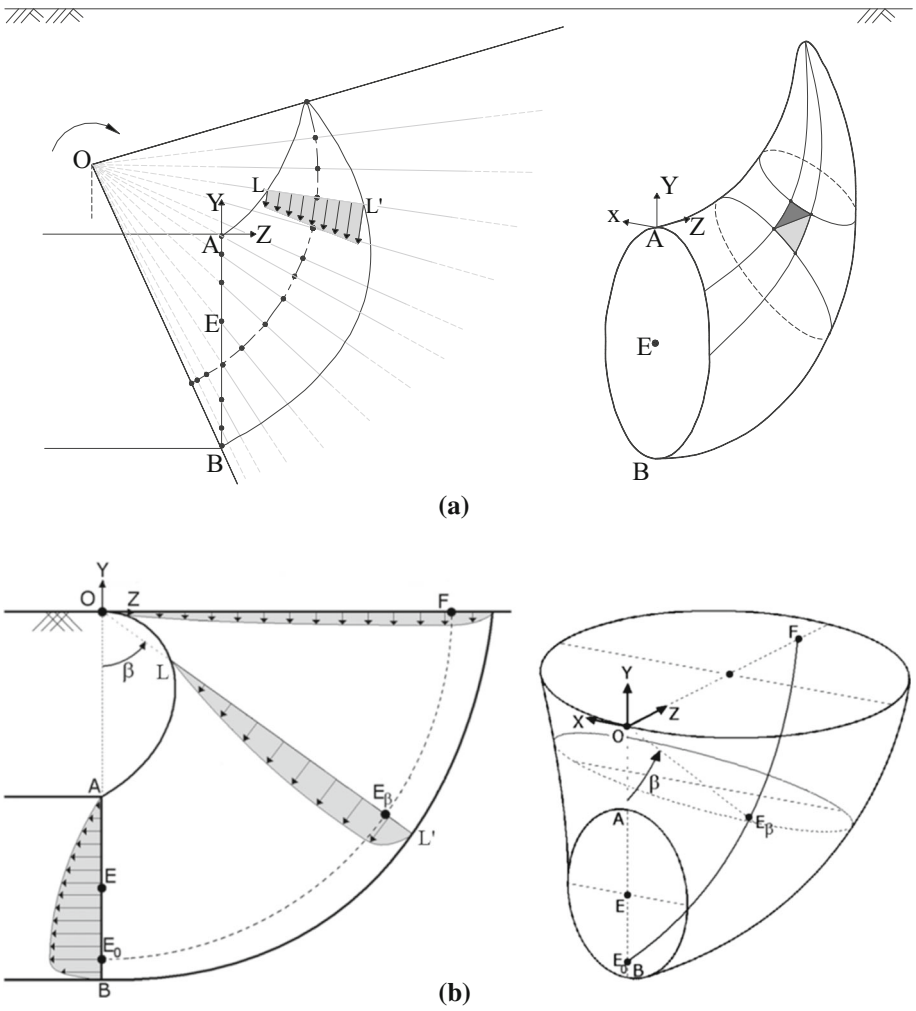

Fig. 1 Sketch of **a** the rigid-block mechanism [26] and **b** the continuous velocity mechanism [28]

collapse mode, the kinematic approach of limit analysis gives a rigorous lower-bound solution to the required face pressure; for the passive blowout mode, a rigorous upper-bound solution can be derived. Therefore, by considering both the collapse and the blowout modes, a range of the necessary face pressures against both failures can be theoretically determined.

However, in the case of the frictional soil, only the collapse failure mechanism gives good predictions compared with other existing solutions as well as numerical modeling results. The blowout failure mechanism leads to very huge estimation (more than 1000 kPa) which is unrealistic in the practical engineering [26, 27]. In the case of the purely cohesive soil, both the collapse and blowout mechanisms produce good estimations on the required face pressure, and a reasonable and effective range can be obtained [27, 28]. Thus, in this work, only the collapse mode is concerned in the case of the frictional soil, and both collapse and blowout modes are taken into account in the case of the purely cohesive soil. Table 1 summaries the failure modes and the failure mechanisms with respect to the soil types adopted in this paper.

3 The lognormal random field

The random field theory is used to model the spatial variability of soil properties, e.g., the cohesion c, the friction angle φ and the unit weight γ. A lognormally distributed random field G_i ($i = c, \varphi, \gamma$) is selected to represent positive soil properties, with the mean value μ_i, the standard deviation σ_i and the autocorrelation distance θ_i. It is assumed that the soil properties, like the cohesion and the friction angle, have similar autocorrelation distances θ in a soil stratum [10, 11]. The lognormally distributed random field can be obtained by transformation from its corresponding standard normal random field (zero mean and unit variance). For convenience, the following equations are for the random field of cohesion c, and the random fields of φ and γ can be dealt with the same formulas. The lognormally distributed random field of cohesion c is given by,

$$G_c(\boldsymbol{x}) = \exp\left[\mu_c^{\ln} + \sigma_c^{\ln} G_c^{\ln}(\boldsymbol{x})\right] \tag{1}$$

where $\boldsymbol{x}$ represents the spatial position, $G_c^{\ln}$ is the standard normal random field, $\mu_c^{\ln}$ and $\sigma_c^{\ln}$ are, respectively, given by,

$$\sigma_c^{\ln} = \sqrt{\ln\left(1 + \sigma_c^2/\mu_c^2\right)} \tag{2}$$

$$\mu_c^{\ln} = \ln \mu_c - \left(\sigma_c^{\ln}\right)^2/2 \tag{3}$$

The spatial variability is characterized by the standard deviation and the autocorrelation distance. In natural deposits, the relation of a certain property between two positions decreases as the separation distance increases, and the correlation in the vertical direction shows much smaller autocorrelation distance than that in the horizontal direction [4]. In the random field theory, a spatial autocorrelation function is used to define the correlation between two arbitrary points. The squared exponential autocorrelation function in a 2D random field, which is the most common one in geotechnical engineering, reads [4, 33]

$$\rho_c = \exp\left\{-\left[\left(\frac{|x_1 - x_2|}{\theta_h}\right)^2 + \left(\frac{|y_1 - y_2|}{\theta_v}\right)^2\right]\right\} \tag{4}$$

where (x_1, y_1) and (x_2, y_2) defines the spatial coordinates of two points; θ_h and θ_v, respectively, denote the horizontal correlation distance and the vertical correlation distance. In this work, 2D random fields were employed. For c–φ soils, this is due to the fact that the rigid-block mechanism uses a 2D rotational velocity field (see line LL' in Fig. 1a). For purely cohesive soils, the continuous velocity field (see line LL' in Fig. 1b) is symmetrical with respect to the vertical symmetry (YOZ) plane of the tunnel.

The standard normally distributed random field $G_c^{\ln}$ can be approximately represented by a M-term K–L expansion:

$$G_c^{\ln}(\boldsymbol{x}) \approx \sum_{j=1}^{M} \sqrt{\lambda_j}\, \xi_j \psi_j(\boldsymbol{x}) \tag{5}$$

in which ξ_j is a set of independent standard normal distribution variables; M is the truncation term of the expansion; λ_j and $\psi_j(\boldsymbol{x})$, respectively, denote the eigenvalues and the eigenfunctions of the autocorrelation function in Eq. (4). Please refer to Phoon and Ching [34] for analytical solutions of eigenvalues and eigenfunctions for the autocorrelation function in Eq. (4). The convergence and the accuracy of a K–L expansion depend on the number of terms M. The determination of M relates to the domain of the random field and the autocorrelation distances. The larger the random field domain and the smaller the

Table 1 Summary of failure modes and failure mechanisms used in this work

Ground conditions	Failure mode		Failure mechanism	
Frictional soils	Collapse mode		Rotational collapse mechanism	
Purely cohesive soils	Collapse mode	Blowout mode	Continuous deformation collapse mechanism	Continuous deformation blowout mechanism

autocorrelation distance, the more the terms required for a given accuracy [13].

It is well recognized that a negative correlation exists between c and φ [10, 15]. A cross-correlation coefficient $\rho_{c,\varphi}$ between the cohesion c and the friction angle φ is considered in this work, and two cross-correlated random c and φ fields can be expressed [10]:

$$G_{\mathrm{c}}(\boldsymbol{x}) \approx \exp\left[\mu_{\mathrm{c}}^{\ln} + \sigma_{\mathrm{c}}^{\ln} G_{\mathrm{c}}^{\ln}(\boldsymbol{x})\right] \tag{6}$$

$$G_{\varphi}(\boldsymbol{x}) \approx \exp\left\{\mu_{\varphi}^{\ln} + \sigma_{\varphi}^{\ln}\left[G_{\mathrm{c}}^{\ln}(\boldsymbol{x})\rho_{c,\varphi}^{\ln} + G_{\varphi}^{\ln}(\boldsymbol{x})\sqrt{1-\left(\rho_{c,\varphi}^{\ln}\right)^2}\right]\right\} \tag{7}$$

where $\rho_{c,\varphi}^{\ln}$ is the cross-correlation coefficient between ln c and ln φ. The relation between $\rho_{c,\varphi}^{\ln}$ and $\rho_{c,\varphi}$ is given by Fenton and Griffiths [12]:

$$\rho_{c,\varphi}^{\ln} = \frac{\ln\left[\left(1+\rho_{c,\varphi}\mathrm{COV}(c)\mathrm{COV}(\varphi)\right)\right]}{\sqrt{\ln\left[1+\mathrm{COV}^2(c)\right]\ln\left[1+\mathrm{COV}^2(\varphi)\right]}} \tag{8}$$

where $\mathrm{COV}(c) = \sigma_{\mathrm{c}}/\mu_{\mathrm{c}}$ and $\mathrm{COV}(\varphi) = \sigma_{\varphi}/\mu_{\varphi}$, respectively, represent the coefficients of variation of the cohesion c and of the friction angle φ.

4 The SPCE/GSA method

4.1 The polynomial chaos expansion

The PCE method is an efficient approach to build an analytical metamodel of the response of a complex mechanical system. A detailed interpretation of the main principles and on how to implement this method can be found in Mollon et al. [25]. In this section, this approach is briefly described as follows.

Consider a computational model T whose input parameters are modeled by independent random variables gathered in an input vector $\boldsymbol{\xi} = \{\xi_1, \xi_2, \ldots, \xi_L\}$, L being the number of the input parameters. The model response Y can be represented by a PCE [36]:

$$Y = T(\boldsymbol{\xi}) \cong \sum_{j=1,\,\boldsymbol{\alpha}\in A}^{P} k_j \psi_{\boldsymbol{\alpha}}(\boldsymbol{\xi}) \tag{9}$$

where $\psi_{\boldsymbol{\alpha}}(\boldsymbol{\xi})$ are the multivariate polynomials and k_j are the unknown coefficients of the PCE. The multivariate polynomial is equal to the products of the univariate polynomials $H_{\alpha_i}(\xi_i)$,

$$\psi_{\boldsymbol{\alpha}}(\boldsymbol{\xi}) = \prod_{i=1}^{L} H_{\alpha_i}(\xi_i) \tag{10}$$

where $\boldsymbol{\alpha} \in \mathbb{N}^L$ is a L-tuple (or multi-indices) that contains a set of integers, $\boldsymbol{\alpha} = (\alpha_1, \ldots, \alpha_i, \ldots, \alpha_L)$, $\alpha_i \in \mathbb{N}$, and α_i is the degree of the univariate polynomial; i indexes the ith variable ξ_i. The univariate polynomials of Eq. (10) are related to the type of the distribution of the input random variables, for instance, the Hermite polynomials for normal (or Gaussian) random variables, Laguerre polynomials for Gamma random variables [31]. The family of multivariate Hermite PC expansions is widely used in geotechnical problems [14–20, 25]. If the input variables are non-normally distributed, the isoprobabilistic transformation can be used to transform them into standard norm variables [36]; if the input variables are correlated, the Nataf transformation or the Cholesky transformation can be used to de-correlate them [18, 25].

For practical application, the PCE is truncated according to the common truncation scheme by which only those multivariate polynomials of total degree less than p are retained in Eq. (9). It leads to the corresponding truncation set $A = \{\boldsymbol{\alpha} \in \mathbb{N}^L\colon\ \boldsymbol{\alpha}_1 = \sum_1^L \alpha_i \le p\}$, and the number of terms in the truncated PCE is equal to

$$P = \mathrm{card}\, A = \frac{(L+p)!}{L!p!} \tag{11}$$

The common truncation scheme is able to deal with small dimension (<5 variables) problems, but it is not practically applicable for high-dimensional ones, like 100–200 random variables arising from the random field discretization. For the purpose of tackling high-dimensional problems, the low-rank truncation scheme [5] and the hyperbolic truncation scheme [7] were proposed. The hyperbolic truncation scheme defines a so-called q-quasi-norm and requires that the q-quasi-norm is not bigger than the order p of the PCE, where the q-quasi-norm reads [7]

$$\|\boldsymbol{\alpha}\|_q = \left(\sum_{i=1}^{M} \alpha_i^q\right)^{1/q} \quad (0<q<1) \tag{12}$$

This hyperbolic truncation scheme leads to the truncate set $A = \{\boldsymbol{\alpha} \in \mathbb{N}^L\colon\ \boldsymbol{\alpha}_q \le p\}$. It can effectively reduce the retained PCE terms compared to the common truncation scheme by limiting the number of high-degree multivariate polynomials. The smaller the value of q is, the less the PCE terms are retained.

4.2 The calculation of the coefficients by the regression approach

The unknown coefficients of the SPCE can be solved by the regression method. Consider an experimental design (ED) $\boldsymbol{\chi}$ with size N, $\boldsymbol{\chi} = [\boldsymbol{\xi}^{(1)}, \boldsymbol{\xi}^{(2)}, \ldots, \boldsymbol{\xi}^{(i)}, \ldots \boldsymbol{\xi}^{(N)}]^{\mathrm{T}}$, $\boldsymbol{\xi}^{(i)} = (\xi_1^{(i)}, \xi_2^{(i)}, \ldots, \xi_L^{(i)})$. The ED is selected randomly by using the Latin Hypercube sampling. Denote by

$\hat{\boldsymbol{Y}} = [\hat{Y}_1, \hat{Y}_2, \ldots, \hat{Y}_N]^{\mathrm{T}}$ the model response corresponding to each set of samples in the ED. Based on the least-square minimization method, the solution to the unknown coefficients of the SPCE reads:

$$\hat{\boldsymbol{k}} = \left(\boldsymbol{\Psi}^{\mathrm{T}}\boldsymbol{\Psi}\right)^{-1}\boldsymbol{\Psi}^{\mathrm{T}}\hat{\boldsymbol{Y}} \tag{13}$$

where $\hat{\boldsymbol{k}} = [\hat{k}_1, \hat{k}_2, \ldots, \hat{k}_P]^{\mathrm{T}}$ represents the column vector of the unknown coefficients of the SPCE and $\boldsymbol{\Psi}$ is a space-independent matrix of dimensions $N \times P$ computed from the basis of the polynomial for each set in the ED. The size N of the ED must ensure that the matrix $\boldsymbol{\Psi}^{\mathrm{T}}\boldsymbol{\Psi}$ is well conditioned. The accuracy of the SPCE can be estimated by the empirical mean-square residual error estimation and the leave-one-out error estimation.

4.3 The stepwise regression technique for a sparse PCE

The sparse PCE is based on two reasons [5]: (a) the low-order interaction terms dominate the model response while the effect of some high-order terms often remains negligible; (2) the input variables may have different contribution to the model response. Thus, two iteration algorithms, the stepwise regression technique [5] and the least angle regression technique [7], were adopted to identify significant PCE terms, further reducing the PCE terms.

In this paper, the stepwise regression algorithm combined with the hyperbolic truncation scheme is employed to build a sparse representation. There are four user-specified parameters in this algorithm, the target accuracy Q^2_{tgt}, the cutoff value $\varepsilon_{\mathrm{cut}}$, the PCE order $p_{\max}$, the so-called norm q. For each PCE order p increasing from 1 to $p_{\max}$, the algorithm consists of two steps: the forward step and the subsequent backward step. In the forward step, it is aimed to select the significant candidate terms from the candidate PCE basis A if it leads to a significant increase in the coefficient of determination R^2, i.e., greater than $\varepsilon_{\mathrm{cut}}$. The candidate PCE basis A is generated according to the hyperbolic truncation scheme (under p and q). In the next backward step, the algorithm discards the negligible terms from the retained PCE basis at the end of the forward step if it leads to an insignificant decrease in R^2, i.e., less than $\varepsilon_{\mathrm{cut}}$. The iteration proceeds until the target accuracy is achieved or the PCE order reaches p. For further details, the authors should refer to Blatman and Sudret [5]. In this work, the four parameters for the algorithm are initialized as: the given accuracy Q^2_{tgt} of 0.999, the cutoff value $\varepsilon_{\mathrm{cut}}$ of 5×10^{-5}, the maximal order $p_{\max}$ of 5 and $q = 0.7$.

4.4 The global sensitivity analysis

The Sobol's indices, widely used for the GSA, can provide the respective effect of each random variable or a group of random variables to the variance of the system response. The Sobol's indices can be analytically computed by using the PCE coefficients [6, 33], and the Sobol's index of a single variable can be calculated by

$$S(\xi_i) = \frac{\sum_{\boldsymbol{\alpha}\in A_i}(k_j)^2 E\left[(\psi_{\boldsymbol{\alpha}})^2\right]}{\sum_{\boldsymbol{\alpha}\in A}(k_j)^2 E\left[(\psi_{\boldsymbol{\alpha}})^2\right]} \tag{14}$$

in which k_j is the PCE coefficients computed by Eq. (13); A represents the obtained truncation set, and A_i, a subset of A, is defined by

$$\begin{aligned} A_i = \{&\alpha = (\alpha_1, \ldots \alpha_i, \ldots, \alpha_L) \in A : \alpha_i > 0, \\ &\alpha_j = 0, 1 \le j \le L, \quad j \ne i\} \end{aligned} \tag{15}$$

and the expectation $E[(\psi_{\boldsymbol{\alpha}})^2]$ is computed by

$$E\left[(\psi_{\boldsymbol{\alpha}})^2\right] = \prod_{i=1,\alpha_i\in A}^{L} \alpha_i! \tag{16}$$

The Sobol's index of a group of variables can be obtained in a similar manner by only changing the subset of A in the numerator in Eq. (14).

4.5 The SPCE/GSA procedure

The PCE/GSA was firstly proposed by Sudret [36] in the GSA. This author suggested a two-step strategy: first finding the most important variables using a low-order PCE (say, second order); then constructing a higher-order PCE (say, fifth order) with the reduced dimension. This procedure was extended by Al-Bittar and Soubra [3] for the probabilistic analysis of computationally expensive models, named as SPCE/GSA.

Even though SPCE is capable to handle high-dimensional problems, the computational time could still be huge, especially for a probabilistic analysis related to a random field. Since different input parameters often have different levels of influence on the model response, the main idea of SPCE/GSA is to identify significant input variables using GSA at first. The GSA is performed by using a second-order PCE to calculate the Sobol's indices of the input variables. It should be noted that the PCE order has almost no influence on the Sobol's indices, so a PCE with order 2 is sufficient to provide the contribution of each input variable to the system response. This GSA makes it possible to reduce the dimension. Al-Bittar and Soubra [3] discarded those input variables with very small Sobol's

indices (a negligible weight in the system response) and suggested that the value of 2% of the Sobol's index of the first most significant input variable is regarded as a threshold, by which only those input variables with Sobol's indices bigger than this threshold are kept, referred to as the 'effective dimension.' In this work, those less important input variables whose Sobol's indices are smaller than this threshold are set to be deterministic at their mean values instead of dropping them, as suggested by Sudret [36]. After reducing the dimension, the second step is to construct the SPCE based on the 'effective dimension.' Figure 2 shows the flowchart for the SPCE/GSA procedure.

4.6 Probabilistic analysis based on the SPCE-metamodel

Once the SPCE coefficients are determined, an analytical metamodel that uses the truncated SPCE to represent the original system response is built. Then, this analytical metamodel can be used to obtain the probabilistic density function (PDF) of the system response with the application of the Monte Carlo simulation (MCS) [25].

In order to assess the failure probability against the tunnel face failure at a given face pressure σ_T, a performance function with respect to the collapse is defined as:

$$G_1 = \sigma_T - \sigma_t \tag{17}$$

A performance function in terms of the blowout is defined as:

$$G_2 = \sigma_t - \sigma_T \tag{18}$$

where σ_T is the applied face pressure and σ_t is the required face pressure calculated by the obtained metamodel, $G_1 < 0$ (or $G_2 < 0$) corresponding to the failure domain. In the subsequent calculations, the applied face pressure σ_T is modeled as a random variable which follows the lognormal distribution with a coefficient of variation equal to 15%. The failure probability can be evaluated by using the MCS:

$$P_f = \frac{1}{J}\sum_{i=1}^{J} I(G_j) \quad j = 1, 2 \tag{19}$$

where J is the number of samples for MCS; $I(G_j)$ is equal to 1 for $G_1 < 0$ (or $G_2 < 0$), otherwise $I(G_1) = 0$ [or $I(G_2) = 0$]. Please note that the probabilistic computations based on the metamodel almost cost no time, even if the size of the MCS population is large. In this work, enough MCS samples using the Latin Hypercube sampling technique are taken to get highly accurate results in all MCSs.

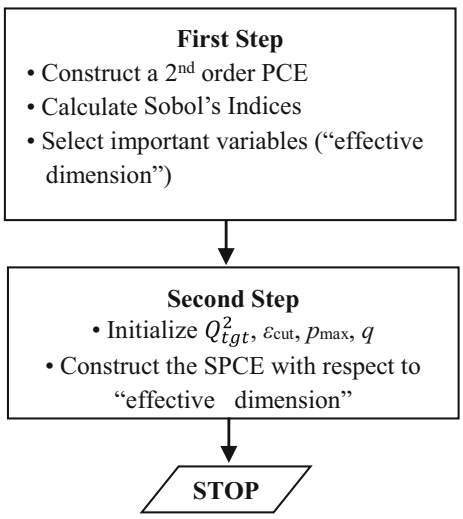

Fig. 2 Flowchart for the SPCE/GSA procedure

5 The probabilistic analysis for the frictional soil

5.1 The problem statement

This section is devoted to apply the SPCE/GSA method to analyze a tunnel face driven in frictional soils in which shear strength parameters are modeled by two random fields. The rotational collapse mechanism proposed by Mollon et al. [26] is effective to compute the required face pressure in this type of soils. Pan and Dias [29] extended this failure mechanism to accommodate the heterogeneous soil, which is used in this work.

Figure 3 presents the longitudinal section of the 3D rotational collapse mechanism for a tunnel face with a diameter D and a buried depth C. Two cross-correlated 2D lognormal random fields are used to model the spatial variability in the horizontal and vertical directions in terms of cohesion c and friction angle φ, bounded by a domain Ω around the tunnel face whose horizontal length and vertical length are, respectively, denoted by l_h and l_v, as shown in Fig. 3. For the realization of the random field, the domain Ω is discretized into rectangular elements, separated by a distance of δ in both the horizontal and vertical directions. The magnitude of the cohesion (or the friction angle) at each grid point on the element can be determined by the K–L expansion. Then, the corresponding value in the center of the element is taken as the average value of those of its four nodes.

The random field in this work is assumed to be anisotropic, since in reality the horizontal correlation distance θ_h is greater than the vertical one θ_v for typical soil stratum [10]. Jiang et al. [15] summarized several previously published articles and recommended that the horizontal correlation distance θ_h ranges between 10 and 40 m, and the vertical correlation distance θ_v between 0.5 and 3.0 m. These recommended ranges are adopted in this work.

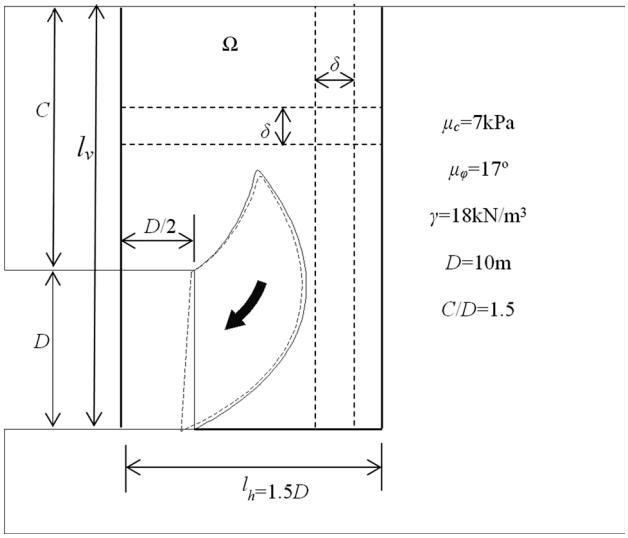

Fig. 3 Sketch of a rigid-block mechanism and the domain of the random field around a tunnel face

Table 2 presents the input parameters used in this work. The tunnel diameter D, the buried depth C, and the soil unit weight γ are taken to be deterministic. With respect to the cross-correlation between c and φ, a negative correlation exists between them. The element size δ is set to 0.5 m, which is fine enough for good results; the horizontal length l_h and vertical length l_v are, respectively, taken as $1.5D$ and $C + D$, as shown in Fig. 3.

5.2 Selection of the truncated order M in a K–L expansion

The K–L expansion always underrepresents the real variance of the random field, and the accuracy of a K–L expansion is correlated with the number of terms M. There are two approaches available for the error estimation on a K–L expansion. The first error estimate based on the variance of the truncated error for a K–L expansion with M terms is given by Phoon and Ching [34]:

$$\varepsilon_1 = \frac{1}{\Omega}\int_{\Omega}\left[1 - \sum_{j=1}^{M}\lambda_j \psi_j^2(\boldsymbol{x})\right]\mathrm{d}\Omega \tag{20}$$

Table 2 Input parameters used in this work

Input variables	Mean value (μ)	COV (%)
c (kPa)	7	20
φ (°)	17	10
γ (kN/m^3)	18	–
C (m)	15	–
D (m)	10	–
σ_T (kPa)	–	15

where Ω is the domain of the random field. This error estimation was used by Ahmed [1] to determine the number of eigenmodes.

As the total variance of $G_c^{\ln}(\boldsymbol{x})$ is decomposed into each term in proportion to eigenvalues λ_j, the approximation is to truncate the K–L expansion up to a desired accuracy using the M largest eigenvalues, see Eq. (5). The ratio of the sum of the M largest eigenvalues to the total sum of all eigenvalues can be taken as a measure of the accuracy of the K–L expansion. Thus, the second error estimation for a K–L expansion is defined as [21]:

$$\varepsilon_2 = 1 - \frac{\sum_{j=1}^{M}\lambda_j}{\sum_{j=1}^{M_T}\lambda_j} \tag{21}$$

where M_T denotes the total number of grid points in the discretized random field, see Figs. 3 and 11 for the discretization of the random fields. This second error estimation was employed by Jiang et al. [13, 14] to determine the value of M.

Figure 4 presents comparisons between these two error estimates ε_1 and ε_2 in the 2D random field for the case of $\theta_h = 40$ m and $\theta_v = 3$ m. It is seen that the error estimate decays quickly with the number of K–L terms. Slight discrepancies in the values of error estimate between ε_1 and ε_2 are observed, but it should point out that the error estimate ε_1 is relatively conservative. Therefore, the first error estimate is used in this paper to determine the number of K–L expansion terms (Fig. 4).

Table 3 lists the K–L terms M for different set of autocorrelation distances considered in this work for a prescribed error of 9–10%. The number of K–L terms increases with the decrease in the autocorrelation distances. Please note that the total number of random variables is equal to $2M$ in the construction of a SPCE, since two random fields are involved.

5.3 The influence of the spatial variability

In this work, the values of the COV of the cohesion and of the friction angle are set as constants, so the spatial variability of the random field is only related to the autocorrelation distances. In order to study the effect of the spatial variability on the PDF of the required face pressure, on the Sobol's index and on the failure probability, the horizontal autocorrelation distance θ_h is set to vary from 10 to 40 m, θ_v from 1.5 to 3.0 m, as listed in Table 3. The cross-correlation coefficient is taken to be zero in all calculations.

5.3.1 The influence on the probability density functions

Figure 5 shows the PDFs of the normalized face pressure corresponding to different autocorrelation distances

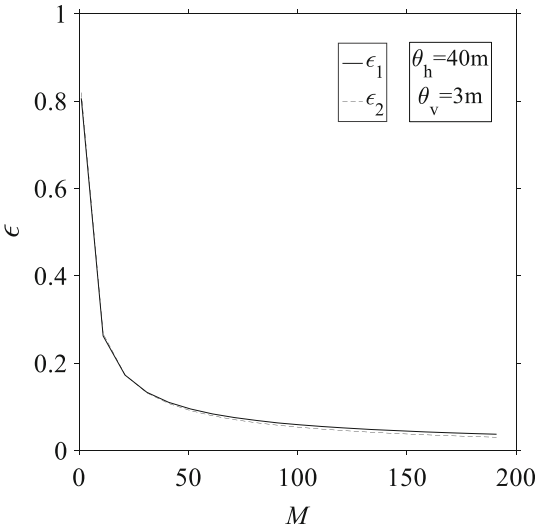

Fig. 4 Comparisons between two error estimates

Table 3 K–L terms for different cases of autocorrelation distances

θ_v (m)	θ_h (m)	M
1.5	10	260
	20	150
	30	120
	40	100
2.0		75
2.5		60
3.0		50

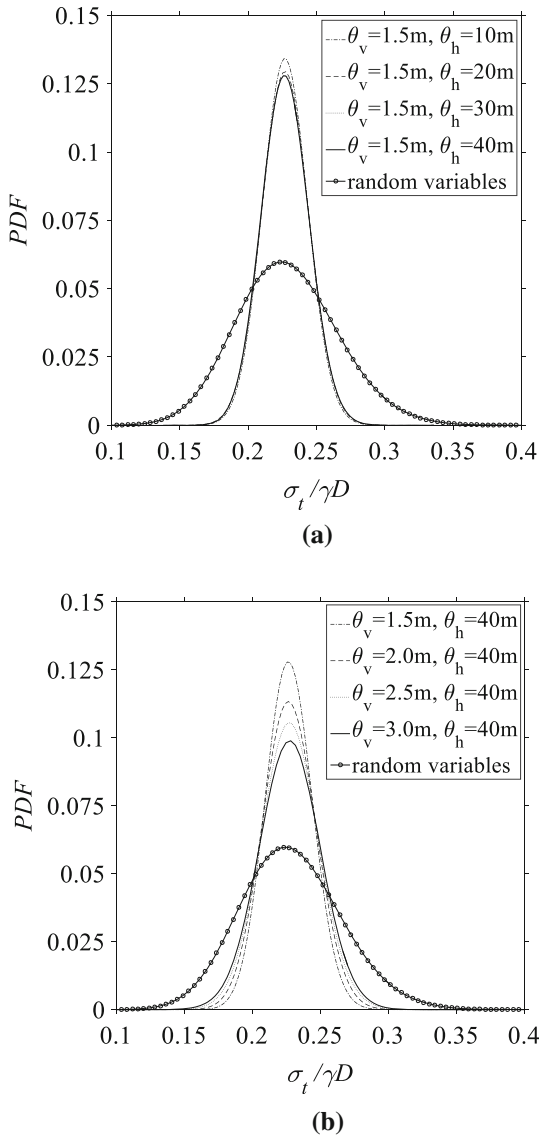

Fig. 5 Influence of spatial variability on the probability density functions

together with the case of random variable. The case of random variable means that the cohesion and the friction angle are considered as random variables. The results are obtained for θ_h ranging between 10 and 40 m with θ_v being 1.5 m in Fig. 5a, and θ_v changing between 1.5 and 3.0 m with $\theta_h = 40$ m for Fig. 5b.

It is seen that a decrease in the autocorrelation distances gives a taller and narrower PDF curve, suggesting that the variability of the required face pressure decreases with the soil spatial heterogeneity (smaller autocorrelation distances generate more severe non-homogeneous soil). A comparison between these two plots shows that the PDF of the required face pressure is more sensitive to the change in the vertical autocorrelation distance.

Besides, it is of high interest to find that the case of random variables produces the most spread-out distribution. This phenomenon was also observed by Fenton and Griffiths [10] and Al-Bittar and Soubra [2] in the study of the bearing capacity of a foundation resting on a spatially random c–φ soil. An interpretation on this phenomenon is as follows. When the autocorrelation distance $\theta \to \infty$ (case of random variables), the soil shear strength tends to be spatially constant in one realization of the random field, but still changes from one realization to another. On the contrary, when the autocorrelation distance $\theta \to 0$, the soil shear strength property field becomes seriously 'rough' in one realization, each discretized element having very different shear strength, but the global average shear strength of the random field changes less than the one of the former case between two realizations. This subsequently leads to smaller variability of the required face pressure.

5.3.2 The influence on the Sobol's index

Figure 6 presents the Sobol's indices of the cohesion c and of the friction angle φ for different autocorrelation distances. It is interesting to see that the autocorrelation

distance hardly influences the Sobol's indices. The Sobol's index of the friction angle φ (around 0.73) is bigger than the one of the cohesion c (around 0.27), which indicates that the friction angle has a more important influence on the required face pressure than the cohesion. This is consistent with the results reported by Mollon et al. [23] in the case of random variables.

5.3.3 The influence on the failure probability

The failure probability as a function of the mean value of applied face pressure is given in Fig. 7 for different autocorrelation distances and for the random variable case. As mentioned above, the applied face pressure σ_T is modeled as a random variable which follows the lognormal distribution with a coefficient of variation equal to 15%.

It is not surprising to find that the failure probabilities are greatly influenced by the applied face pressure, small applied face pressure resulting in very high failure probability. Besides, it can be seen that the increase in the autocorrelation distance leads to an increase in the failure probability, for both the horizontal and vertical autocorrelation distances. For example, the failure probability increases from 3.94×10^{-4} to 7.29×10^{-4} as θ_v increases from 1.5 to 3 m when $\theta_h = 40$ m and $\mu_{\sigma T}/\gamma D = 0.4$. In other words, an overestimation of the autocorrelation distance (or an underestimation of the spatial variation) leads to conservative results in the engineering design. It is also noticed that the vertical autocorrelation distance impacts the failure probability more than the horizontal autocorrelation distance. These conclusions agree with those reported by Jiang et al. [15] who computed the failure

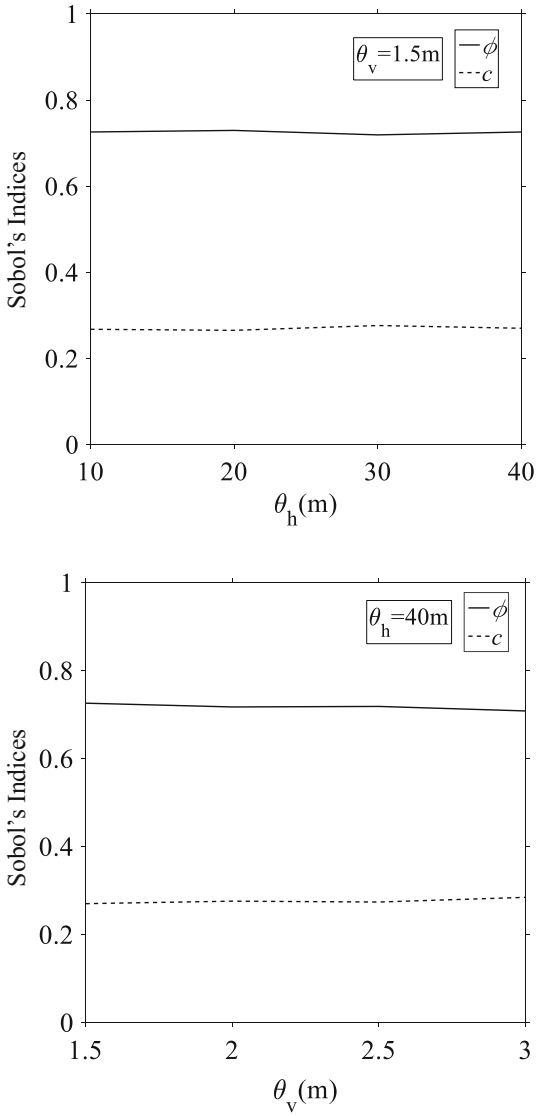

Fig. 6 Influence of spatial variability on the Sobol's indices

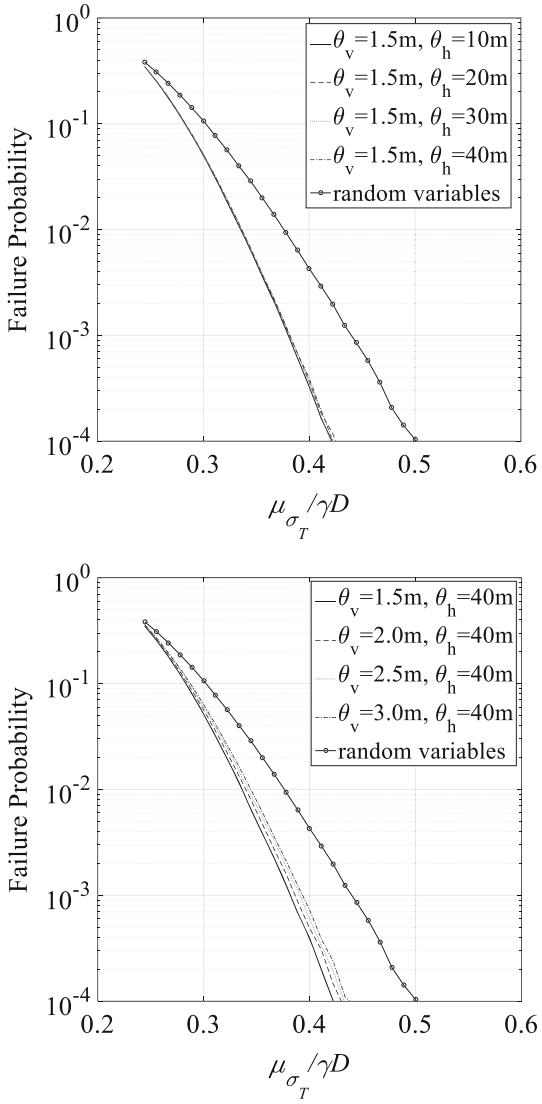

Fig. 7 Failure probability versus the applied face pressure for different soil spatial variabilities

probability of a slope in spatially variable soils. What is more interesting is the observation that the random variables model leads to a much greater failure probability than the case of the random field model in all cases. For instance, the failure probability is equal to 4.3×10^{-3} ($\mu_{\sigma T}/\gamma D = 0.4$) for the random variables model. This implies that neglecting the soil spatial variability and using the random variables model would lead to a much safer but very uneconomic design in the considered cases.

5.4 The influence of the cross-correlation coefficients

In order to discuss the influence of the cross-correlation coefficients, four cases of correlation coefficients ranging from -0.6 to 0.0 are considered. The autocorrelation distances are set to $\theta_v = 3.0$ m and $\theta_h = 40$ m for all the cases. The obtained results of PDFs are given in Fig. 8. This figure shows that the negative cross-correlation $\rho_{c,\varphi}$ leads to a taller and narrower PDF (less variability of the required face pressure). With respect to the random variables case, similar results are observed.

Figure 9 shows the failure probability as a function of the mean value of the applied face pressure for four different correlation coefficients. One can observe that the cross-correlation $\rho_{c,\varphi}$ greatly influences the failure probability. The failure probability decreases with the negative cross-correlation getting stronger. For instance, the failure probability increases from 3.41×10^{-4} to 7.29×10^{-4} as $\rho_{c,\varphi}$ changes from -0.6 to 0.0 at $\mu_{\sigma T}/\gamma D = 0.4$ in the random field results, rising from 1.06×10^{-3} to 4.30×10^{-3} in the random variable results. It can be concluded that neglecting the negative cross-correlation between c and φ

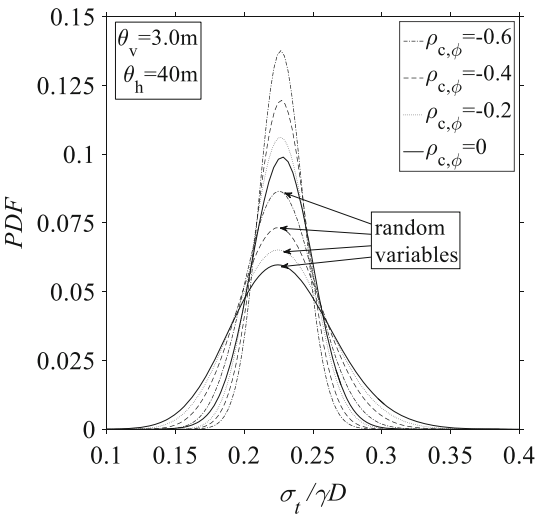

Fig. 8 Influence of correlation coefficients on the probability density functions

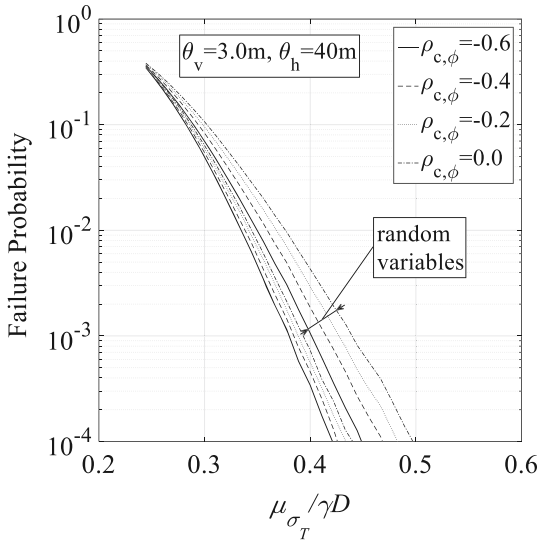

Fig. 9 Failure probability versus applied face pressure under different correlation coefficients

leads to a conservative design. A same conclusion was reported by Mollon et al. [23] and Jiang et al. [15]. In addition, the observation that the random variable model gives much more conservative results compared with the random field model is found again.

Figure 10 presents the influence of the cross-correlation coefficients on the Sobol's indices. One can see that the Sobol's index is greatly influenced by the cross-correlation coefficient; the Sobol's index of φ decreases as the cross-correlation becomes weak, while the Sobol's index of c shows an opposite trend. However, the total Sobol's index of c and φ keeps unchanged and is close to 1 in all cases.

6 Probabilistic analysis of purely cohesive soils

6.1 The problem statement

This section aims to analyze a tunnel face driven in purely cohesive soils in which the undrained shear strength c_u and the soil unit weight γ are modeled by two random fields. The collapse and blowout face pressure obtained by these two continuous velocity fields agree well with those provided by numerical calculations, but with higher computation efficiency. These two continuous deformation mechanisms are extended in this work to consider the influence of the spatial variability of the cohesion and of the unit weight.

Figure 11 presents the longitudinal section of the continuous deformation mechanism for a tunnel face with a diameter D and a buried depth C. Two independent 2D lognormal random fields are adopted to model the spatial variability in the horizontal and vertical directions in terms

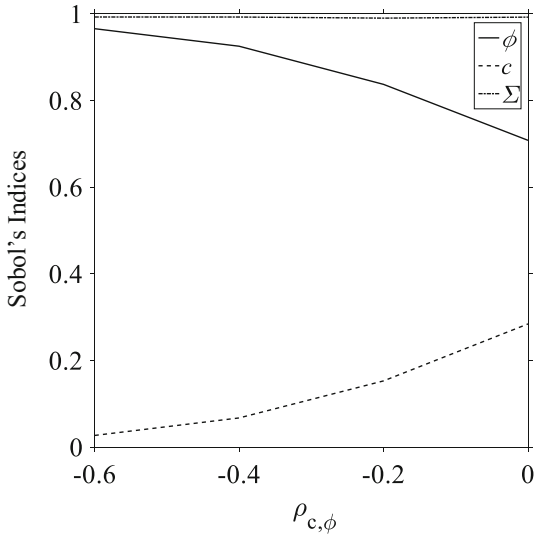

Fig. 10 Influence of correlation coefficients on the Sobol's indices

of the cohesion c and the unit weight γ. The domain of the random field is denoted by Ω ahead of the tunnel face, as shown in Fig. 11. A similar scheme as the frictional soil case is used to discretize the random field.

Table 4 presents values of input parameters used in this work. The tunnel diameter D and the buried depth C are taken to be deterministic. No cross-correlation between c and γ is considered. Only two cases of autocorrelation distances are taken as $\theta_v = 1.5$ m, $\theta_h = 20$ m and $\theta_v = 3.0$ m, $\theta_h = 40$ m in this section, which, respectively, corresponds to 270 and 70 terms to be retained in a K–L expansion for a target error of 9–10%.

6.2 Influence on the probability density functions

Figure 12 shows the PDFs of the normalized face pressure corresponding to the collapse mode and to the blowout mode. Two cases of autocorrelation distances are considered. The left curves refer to the collapse mode, and the right hand to the blowout mode. It is observed that the

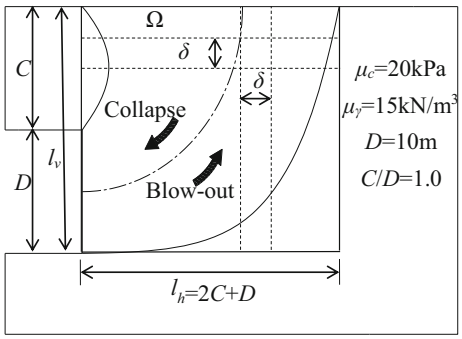

Fig. 11 Continuous deformation mechanism and domain of the random field around a tunnel face

Table 4 Input parameters used in this work

Input variables	Mean value (μ)	COV (%)
c (kPa)	20	20
γ (kN/m^3)	15	5
C (m)	10	–
D (m)	10	–
σ_T (kPa)	–	15

blowout curves correspond to larger face pressures than those of collapse curves. Similarly to the case of frictional soils, the high autocorrelation distance leads to shorter and wider PDF curves.

6.3 Influence on the Sobol's indices

Figure 13 presents the corresponding Sobol's indices for the collapse mode and blowout mode. It can be again observed that the autocorrelation distance has a negligible influence on the Sobol's index. In the studied case, the cohesion c contributes more to the model response than the unit weight γ in terms of both the collapse and the blowout modes. Except for the influence of the computational model, the fact that the COV(c) is four times the magnitude of the COV(γ) may be one reason for this.

6.4 Influence on the failure probability

Figure 14 shows the failure probability versus the mean values of applied face pressure $\mu_{\sigma T}$. The results of two cases of autocorrelation distances together with the random variable model are provided in terms of the collapse failure

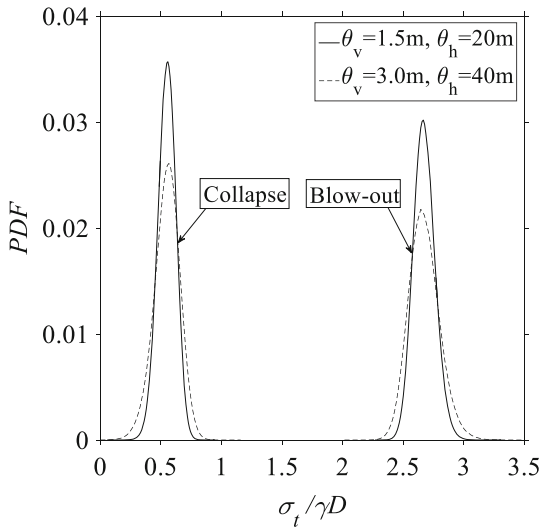

Fig. 12 Probability density functions for the collapse and the blowout modes

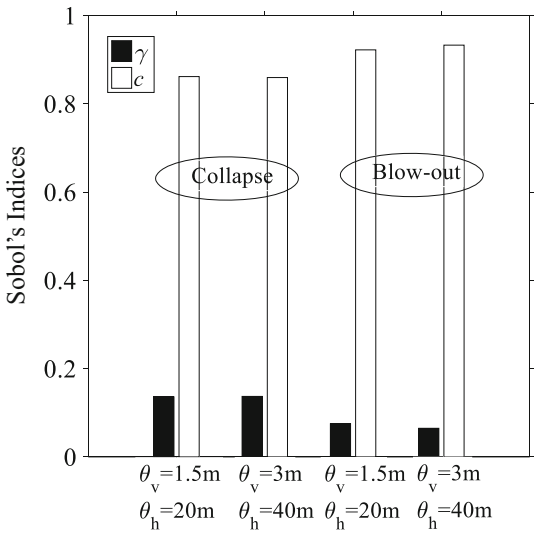

Fig. 13 Sobol's indices for the collapse and blowout failure modes

and blowout failure. The curves at the left-hand side correspond to the collapse mode, and at the right-hand side to the blowout mode.

It is to be expected that the failure probabilities are largely influenced by the applied face pressure. Take the case of $\theta_v = 1.5$ m and $\theta_h = 20$ m as an example, when $\mu_{\sigma T}$ is small the failure probability of collapse is very high. As the applied face pressure increases (before $1.1\gamma D$), the collapse failure probability decreases. In this range, the blowout probability is negligible (smaller than 10^{-4}) and the collapse failure is dominant. When it reaches $1.5\gamma D$, the failure probability of blowout becomes more and more significant and the collapse failure probability is negligible (smaller than 10^{-4}). Then, blowout dominates the tunnel face failure.

In the center of the figure, there exists a range of the applied face pressure ($1.1–1.5\gamma D$) among which the failure probabilities (with respect to the collapse and blowout) are lower than 10^{-4} for the random field model. Such a special range is practically useful for the practical engineering design since it permits to give safe face pressures against both the collapse and blowout considering a target failure probability of 10^{-4}. It is interesting to see that the width of this safe range reduces with the increase in the autocorrelation distance. The random variable assumption fails to give such a safe range, due to the fact that the collapse probability and the blowout probability curves encounter each other before reaching the value of 10^{-4}. The failure probability curve for random variable plotted in Fig. 14 is the sum of the failure probabilities of the two failure modes. This no-safe-range phenomenon is probably because that the random variable model gives conservative results.

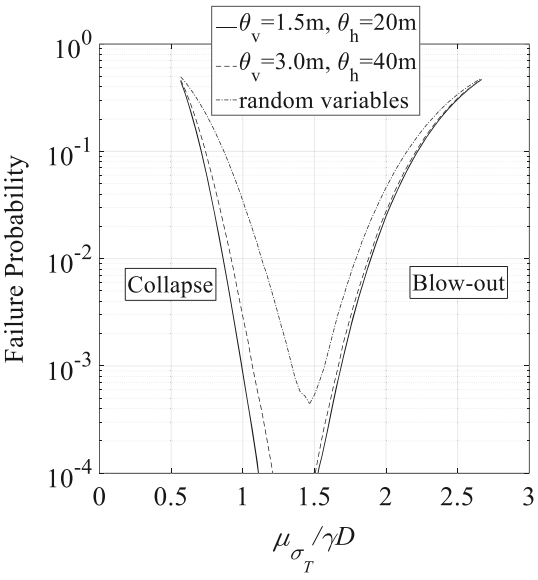

Fig. 14 Failure probability versus applied face pressure

7 Conclusions

A probabilistic analysis is performed on a tunnel face by considering the spatial soil variability. Two sets of 3D failure mechanisms are used to calculate the required face pressure with respect to a frictional soil and a purely cohesive soil in the context of the upper-bound limit analysis. The SPCE-based MCS method is employed to carry out the probabilistic analysis. In the case of frictional soils, the cohesion and the friction angle are modeled as two anisotropic cross-correlated lognormal random fields; with respect to the purely cohesive soil, the cohesion and unit weight are modeled as two independent lognormal random fields. The different levels of the spatial variability and the cross-correlation (in the case of the frictional soils) are considered to study their influence on the probability density function, on the sensitivity index and on the failure probability.

In the case of frictional soils, only the collapse mode is considered. It is shown that the spatial variability has a significant influence on the probability density function as well as on the failure probability, but its effect on the sensitivity index is rather limited. The results indicate that the variability of the required face pressure decreases with the soil spatial heterogeneity, and the failure probability increases with the increase in the autocorrelation distances and with the decrease in the negative correlation between the cohesion and the friction angle. The sensitivity analysis shows that the friction angle is more important than the cohesion.

In the case of the purely cohesive soils, both the collapse and blowout are involved. The influence of spatial variability gives similar results as the frictional soil case. The sensitivity analysis shows that the cohesion is more important than the unit weight. A useful range of the face pressure among which the failure probabilities with respect to both the collapse and the blowout failure modes are lower than a target safety level of 10^{-4} is obtained in this case.

Acknowledgements The first author thanks the China Scholarship Council for providing him with a Ph.D. Scholarship for his research work, and the financial support by the National Basic Research 973 Program of China (2013CB036004) is also greatly appreciated.

References

1. Ahmed A (2012) Simplified and advanced approaches for the probabilistic analysis of shallow foundations. Doctoral dissertation, Nantes
2. Al-Bittar T, Soubra A-H (2013) Bearing capacity of strip footings on spatially random soils using sparse polynomial chaos expansion. Int J Numer Anal Methods Geomech 37(13):2039–2060
3. Al-Bittar T, Soubra A-H (2014) Efficient sparse polynomial chaos expansion methodology for the probabilistic analysis of computationally-expensive deterministic models. Int J Numer Anal Methods Geomech 38(12):1211–1230
4. Baecher GB, Christian JT (2005) Reliability and statistics in geotechnical engineering. Wiley, Hoboken
5. Blatman G, Sudret B (2010) An adaptive algorithm to build up sparse polynomial chaos expansions for stochastic finite element analysis. Probab Eng Mech 25(2):183–197
6. Blatman G, Sudret B (2010) Efficient computation of global sensitivity indices using sparse polynomial chaos expansions. Reliab Eng Syst Saf 95(11):1216–1229
7. Blatman G, Sudret B (2011) Adaptive sparse polynomial chaos expansion based on least angle regression. J Comput Phys 230(6):2345–2367
8. Chen RP, Tang LJ, Yin XS, Chen XM, Bian XC (2015) An improved 3D wedge-prism model for the face stability analysis of the shield tunnel in cohesionless soils. Acta Geotech 10(5):683–692
9. Ibrahim E, Soubra AH, Mollon G, Raphael W, Dias D, Reda A (2015) Three-dimensional face stability analysis of pressurized tunnels driven in a multilayered purely frictional medium. Tunn Undergr Sp Technol 49:18–34
10. Fenton GA, Griffiths D (2003) Bearing-capacity prediction of spatially random c φ soils. Can Geotech J 40(1):54–65
11. Fenton GA, Griffiths DV, Williams MB (2005) Reliability of traditional retaining wall design. Geotechnique 55(1):55–62
12. Fenton GA, Griffiths DV (2008) Risk assessment in geotechnical engineering. Wiley, Hoboken
13. Huang S, Quek ST, Phoon KK (2001) Convergence study of the truncated Karhunen–Loeve expansion for simulation of stochastic processes. Int J Numer Methods Eng 52(9):1029–1043
14. Huang S, Liang B, Phoon KK (2009) Geotechnical probabilistic analysis by collocation-based stochastic response surface method: an Excel add-in implementation. Georisk 3(2):75–86
15. Jiang S, Li D, Cao Z, Zhou C, Phoon KK (2014) Efficient system reliability analysis of slope stability in spatially variable soils using Monte Carlo simulation. J Geotech Geoenviron Eng 141(2):04014096
16. Jiang S, Li D, Zhang L, Zhou C (2014) Slope reliability analysis considering spatially variable shear strength parameters using a non-intrusive stochastic finite element method. Eng Geol 168:120–128
17. Jin-Feng Z, Yu S (2015) Theoretical solutions of a circular tunnel with the influence of the out-of-plane stress based on the generalized Hoek–Brown failure criterion. Int J Geomech 16(3):06015006
18. Li D, Chen Y, Lu W, Zhou C (2011) Stochastic response surface method for reliability analysis of rock slopes involving correlated non-normal variables. Comput Geotech 38(1):58–68
19. Li D, Jiang S, Chen Y, Zhou C (2014) Reliability analysis of serviceability performance for an underground cavern using a non-intrusive stochastic method. Environ Earth Sci 71(3):1169–1182
20. Li D, Zheng D, Cao Z, Tang X, Phoon KK (2016) Response surface methods for slope reliability analysis: review and comparison. Eng Geol 203:3–14
21. Laloy E, Rogiers B, Vrugt JA, Mallants D, Jacques D (2013) Efficient posterior exploration of a high-dimensional groundwater model from two-stage Markov chain Monte Carlo simulation and polynomial chaos expansion. Water Resour Res 49(5):2664–2682
22. Mao N, Al-Bittar T, Soubra AH (2012) Probabilistic analysis and design of strip foundations resting on rocks obeying Hoek–Brown failure criterion. Int J Rock Mech Min Sci 49:45–58
23. Mollon G, Dias D, Soubra AH (2009) Probabilistic analysis and design of circular tunnels against face stability. Int J Geomech 9(6):237–249
24. Mollon G, Dias D, Soubra AH (2009) Probabilistic analysis of circular tunnels in homogeneous soil using response surface methodology. J Geotech Geoenviron Eng 135(9):1314–1325
25. Mollon G, Dias D, Soubra AH (2010) Probabilistic analysis of pressurized tunnels against face stability using collocation-based stochastic response surface method. J Geotech Geoenviron Eng 137(4):385–397
26. Mollon G, Dias D, Soubra AH (2011) Rotational failure mechanisms for the face stability analysis of tunnels driven by a pressurized shield. Int J Numer Anal Methods Geomech 35(12):1363–1388
27. Mollon G, Dias D, Soubra AH (2013) Range of the safe retaining pressures of a pressurized tunnel face by a probabilistic approach. J Geotech Geoenviron Eng 139(11):1954–1967
28. Mollon G, Dias D, Soubra AH (2013) Continuous velocity fields for collapse and blowout of a pressurized tunnel face in purely cohesive soil. Int J Numer Anal Methods Geomech 37(13):2061–2083
29. Pan Q, Dias D (2015) Face stability analysis for a shield-driven tunnel in anisotropic and nonhomogeneous soils by the kinematical approach. Int J Geomech 16(3):04015076
30. Pan Q, Dias D (2016) The effect of pore water pressure on tunnel face stability. Int J Numer Anal Methods Geomech 40(15):2123–2136
31. Pan Q, Dias D (2017) Upper-bound analysis on the face stability of a non-circular tunnel. Tunn Undergr Sp Technol 62:96–102
32. Phoon KK, Huang SP (2007) Uncertainty quantification using multi-dimensional hermite polynomials. In: Probabilistic applications in geotechnical engineering (GSP 170). Geotechnical Special Publication, ASCE, Reston, VA, pp 1–10. doi:10.1061/40914(233)12
33. Phoon KK (ed) (2008) Reliability-based design in geotechnical engineering: computations and applications. CRC Press, Boca Raton
34. Phoon KK, Ching J (eds) (2014) Risk and reliability in geotechnical engineering. CRC Press, Boca Raton

35. Senent S, Mollon G, Jimenez R (2013) Tunnel face stability in heavily fractured rock masses that follow the Hoek–Brown failure criterion. Int J Rock Mech Min Sci 60:440–451
36. Sudret B (2008) Global sensitivity analysis using polynomial chaos expansions. Reliab Eng Syst Saf 93(7):964–979
37. Soubra AH, Mao N (2012) Probabilistic analysis of obliquely loaded strip foundations. Soils Found 52(3):524–538
38. Tang XW, Liu W, Albers B, Savidis S (2014) Upper bound analysis of tunnel face stability in layered soils. Acta Geotech 9(4):661–6718
39. Zeng P, Senent S, Jimenez R (2014) Reliability analysis of circular tunnel face stability obeying Hoek–Brown failure criterion considering different distribution types and correlation structures. J Comput Civ Eng 30(1):04014126